

Article

Effect of the Cu/Mg Ratio on Mechanical Properties and Corrosion Resistance of Wrought Al–Cu–Mg–Ag Alloy

Talal Talib Alshammari *, Muhammad Farzik Ijaz , Hamad F. Alharbi  and Mahmoud S. Soliman 

Mechanical Engineering Department, College of Engineering, King Saud University, P.O. Box 800, Riyadh 11421, Saudi Arabia; mijaz@ksu.edu.sa (M.F.I.); harbihf@ksu.edu.sa (H.F.A.); solimanm@ksu.edu.sa (M.S.S.)

* Correspondence: talaltalib6@gmail.com

Abstract: The present study aimed to investigate the influence of magnesium (Mg) on the mechanical properties and corrosion behavior of wrought Al–4Cu–xMg–0.6Ag alloys. The results from Optical Microscope, SEM, XRD analysis, and Thermo-Calc simulation were used to identify the microstructure formed after the aging process. Testing for hardness and tensile strength was conducted, in addition to corrosion testing. It was found that Mg significantly impacts the hardness of the alloys, with a high Mg content (low Cu/Mg ratio) increasing the hardness but reducing the tensile strength and ductility. This study attributed this to the formation of the S phase, which is dependent on both the quantity in the bulk and the size of the phase. The grain size was found to be finer with a higher Mg content, since the particle size inhibits grain growth during the artificial aging process. Counterintuitively, the corrosion activity was reduced in the high-Mg-content alloy due to its large particle size and the reduced galvanic cell effect. This study highlighted the importance of considering the effects of Mg on the mechanical properties and corrosion behavior of Al–Cu–Mg–Ag alloys.

Keywords: Al–Cu alloys; Thermo-Calc; S phase; corrosion; Mg effect



Citation: Alshammari, T.T.; Ijaz, M.F.; Alharbi, H.F.; Soliman, M.S. Effect of the Cu/Mg Ratio on Mechanical Properties and Corrosion Resistance of Wrought Al–Cu–Mg–Ag Alloy. *Crystals* **2023**, *13*, 908. <https://doi.org/10.3390/cryst13060908>

Academic Editor: Bolv Xiao

Received: 11 April 2023

Revised: 14 May 2023

Accepted: 26 May 2023

Published: 2 June 2023



Copyright: © 2023 by the authors. Licensee MDPI, Basel, Switzerland. This article is an open access article distributed under the terms and conditions of the Creative Commons Attribution (CC BY) license (<https://creativecommons.org/licenses/by/4.0/>).

1. Introduction

Aluminum alloys containing small amounts of copper and magnesium alloying elements (usually denoted as Al–Cu–Mg alloys) are widely used in many important transport applications including the aerospace and automobile industries. The high usage of this category of aluminum alloys is mainly related to their great properties, such as a light weight, high strength, high corrosion resistance, high ductility, and high strength-to-weight ratio. Further, the different types of possible pre-thermomechanical treatments can significantly improve the mechanical properties of these alloys (e.g., tensile strength improves from 190 to 430 MPa by aging), making them suitable for various applications [1]. In particular, the presence of a slight weight percentage of Cu (~4.0 wt.%) and Mg (~1.0 wt.%) in these alloys improves the precipitation hardening through aging heat treatment.

The precipitation hardening in Al–Cu–Mg alloys usually increases the hardness and strength of the material. The aging treatment facilitates the formation of various precipitates in these alloys depending on the composition, temperature, aging time, and other processing conditions [2,3]. In the aging treatment of an Al–Cu–Mg alloy, the process starts with the formation of a supersaturated solid solution (SSS) where all the small phases dissolve in the more abundant α -aluminum phase. This is performed by heating the Al–Cu–Mg alloy to approximately 520 °C to form a homogeneous solid solution, followed by rapid quenching in water. The alloy is then heated (artificial aging) to a moderate temperature, approximately 180 °C, to facilitate the formation of stable precipitates in the matrix (α) phase. In an Al–Cu–Mg alloy, the type of stable precipitates is strongly influenced by the atomic ratio of Cu to Mg. For alloys of low Cu/Mg ratios, with compositions in the (α + S) phase field at approximately 190 °C, the stable precipitate is the S (Al₂CuMg) phase [4]. The

formation of this precipitate phase at equilibrium is typically preceded by several intermediate stages: the Guinier Preston Bagaryatsky (GPB) zone, S'' , and S' (i.e., the series is $SSS \rightarrow GPB \rightarrow S'' \rightarrow S' \rightarrow S$) [5]. However, for Al–Cu–Mg alloys with high Cu/Mg ratios having compositions in the $(\alpha + \theta + S)$ phase field at 190 °C, the equilibrium precipitate is the θ (Al_2Cu) phase, and its precursors are GPB, θ'' , and θ' ($SSS \rightarrow GPB \rightarrow \theta'' \rightarrow \theta' \rightarrow \theta$) [5–7]. It should be noted that the intermediate metastable phases have noticeable effects on the different stages of the aging hardening response.

The formation of stable precipitates and their precursors in the matrix aluminum (α) phase during aging hardening enhances the mechanical properties of Al–Cu–Mg alloys. The general mechanism of precipitation hardening is that the dislocations nucleate from vacancies and try to move through the precipitates during plastic deformation, while the precipitates resist their motion. There are two common ways for the dislocations to move, either dislocation cuts through the precipitate or moves around the precipitate particles. Moreover, the backup of dislocations around precipitates can further impede the motion of dislocations due to the interactions between new and current dislocations [5]. Therefore, an increase in stress is required for the motion of dislocations in the presence of precipitate particles in Al–Cu–Mg alloys. The morphology of precipitates and their distribution in the matrix can strongly affect the percentage increase in hardening and strength.

Many studies showed the effect of various possible precipitates on the mechanical performance of Al–Cu–Mg alloys [8,9]. For instance, Liu et al. [10] studied the Cu/Mg ratio influence on the mechanical properties using a 2519 alloy (high Cu/Mg ratio) and a 2024 alloy (low Cu/Mg ratio). According to this investigation, if the ratio of Cu/Mg decreased, the hardening and mechanical properties improved. The Cu/Mg ratio of 3.41 in the 2024 alloy resulted in a hardness of 152 HV, while the 2519 alloy, with a Cu/Mg ratio of 16.29, had a hardness of 141 HV. The authors compared the age hardening of different Al–Cu–Mg alloys with high and low Cu/Mg ratios and found that the best ratio for improved hardening is ~ 7.85 ; by designing and testing a new alloy, they found that the θ' phase changed to the S phase, which improves the mechanical property.

The addition of the silver (Ag) element to Al–Cu–Mg alloys has attracted increasing attention owing to its further improvement in strength, thermal stability, and creep resistance [1,3,11,12]. The addition of a small amount of the Ag element to the ternary alloy (Al–Cu–Mg) helps to form a new precipitate phase, called Ω , that lies on the (111) α plane of the α phase [13–16]. It should be noted that the (111) α plane is the dominant slip plane of aluminum. Therefore, it is widely acknowledged that the Ω precipitates in Al–Cu–Mg–Ag alloys have more resistance to dislocation motion as they lie on the main (111) α deformation slip plane of aluminum, compared to other precipitates such as, for example, the S precipitates formed on the (210) α plane [4,17]. The Ω phase is usually formed as hexagon plates with thicknesses of 2–3 nm parallel to the (111) α planes [18]. The Ω phase can be uniformly distributed in the matrix if the alloy is homogenized [2]. Instead of heterogeneous nucleation, the nucleation of the Ω phase begins at the locations where Mg–Ag co-clusters are present [19,20]. The amounts of Ag and Mg and the number of Mg–Ag co-clusters were found to strongly affect the number density of the Ω phase that can be formed in the matrix [21,22]. There is usually a competition between the formation of the Ω phase and other precipitates such as the θ' or S' phases, depending on the amount of Mg in the alloy ($\alpha + \theta + S$ or $\alpha + S$ at high or low Cu/Mg ratios, respectively) [4,19,23]. Chen et al. [17] studied the ratio of Cu/Mg by controlling Cu and Ag, and they found that increasing the Mg concentrations promoted the Ω precipitates. A low Cu/Mg ratio enhanced the Mg–Ag co-cluster, which led to more Ω precipitates, while a high Cu/Mg ratio enhanced the S precipitates [4,17]. Ringer et al. [24] found that the Mg–Ag co-cluster effectively acted as a nucleation site for the formation of Ω precipitates. Decreasing the Cu/Mg ratio enhanced the Ω precipitates by increasing the Mg concentration.

Changing the Mg concentration in the composition led to the same change in corrosion resistance, as mentioned in the following literature. By adding small amounts of Ag and Mg to an Al–Cu alloy, the volta potential of the Al matrix was shifted to a higher positive

value. This results in a reduction in the potential differences (from 190 to 110 mV) between the coarse Al_2Cu particles and the Al matrix, as well as a weakening of the activity of the galvanic corrosion couple, where the pitting corrosion resistance increased [25]. As the Mg content increased, the corrosion current density also increased, indicating a corresponding increase in the corrosion rate of the Al–Cu–Mg–Ag alloy. This could potentially be linked to the greater potential difference between the PFZ and the matrix [26]. The self-corrosion potential of the Al–Cu–Mg–Ag alloy was evaluated using PFZ, and it was found that $\text{EPFZ} < \text{Eq} < \text{EMatrix}$. By adjusting the grain boundary microstructure, T614 temper can significantly enhance the exfoliation corrosion resistance of the alloy [27]. Intermetallic particles found in aluminum alloys have a significant impact on the breakdown of the passivity and pit morphology of these alloys when exposed to seawater.

The present study investigates the effects of increasing Mg concentration from 0.4 to 1.4 wt.% in Al–4%Cu–xMg–0.6%Ag alloy. The discussion of this study focuses on the mechanical properties, microstructure, and corrosion resistance.

2. Materials and Methods

The methodology for this study aims to examine the effects of Cu/Mg ratios on the mechanical properties and corrosion resistance of Al–Cu–Mg–Ag alloys. The materials were designed to present high and low Cu/Mg ratios, as shown in Figure 1. The change in Cu/Mg was controlled by increasing the Mg content while keeping the Cu and Ag fixed at the same percentage. The Mg concentration was raised from 0.4 to 1.4 wt.%, where the ratios were 10%, called high, and 3%, called low. This change in Mg content was based on the Al–Cu–Mg phase diagram, which predicts that a high Cu/Mg ratio could result in the presence of three phases ($\alpha + \theta + \text{S}$) with different percentages of phases [11].

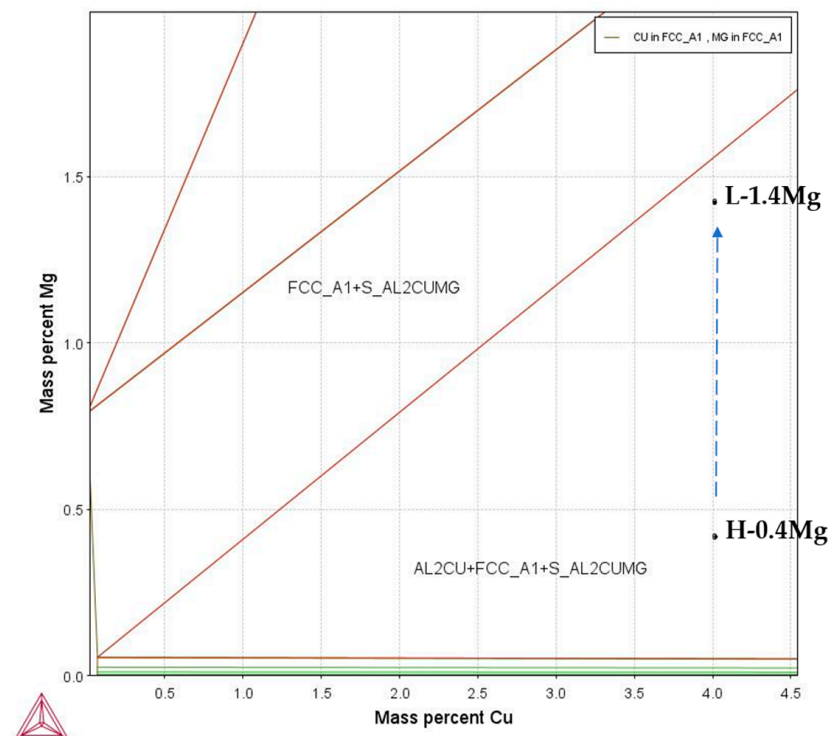


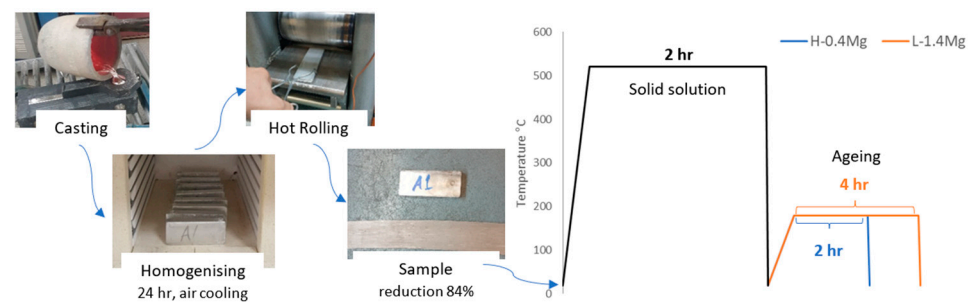
Figure 1. Al–Cu–Mg phase diagram at 180 °C.

The alloys were prepared from pure bulk elements melted at 730 °C and cast into heated mold of steel at 450 °C. The resulting ingots were then homogenized at 520 °C for 24 h, followed by furnace cooling [28]. The chemical composition of the ingots was analyzed using SPECTRO MAXx Spectral analyzer, and the results are shown in Table 1.

Table 1. The chemical composition analysis by SPECTROMAXx Metal Analyzer.

Samples	Composition (wt.%)				Cu/Mg Ratio
	Al	Cu	Mg	Ag	
H-0.4Mg	94.94	3.95	0.4	0.71	9.88
L-1.4Mg	93.73	4.23	1.43	0.61	2.96

The casted ingots were then rolled from 16mm to 2.5 mm in thickness by hot rolling machine, which resulted in an 84% reduction, forming the alloy sheets. These sheets were then solution-treated at 520 °C and quenched in water at room temperature, inducing the formation of a supersaturated solid solution (SSS). Afterwards, the samples were aged in a salt bath at 180 °C to determine the aging peak point for hardness [28,29], as shown in Figure 2. A hardness test, Vickers hardness type, was performed on the scale of 10 KgF during the 15 s. The hardness was determined by taking an average of 5 indents at a random location on the sample. Tensile samples were then cut using an Electric Discharge Machine (EDM) from the SSS sheets, according to ASTM E 8/E 8M-08 standards. The tensile samples were then aged at the previously determined hardness peak point and were tested using an INSTRON universal testing machine at a strain rate of 10^{-3} s^{-1} . To ensure accuracy, three samples were tested for each alloy to verify the outcomes.

**Figure 2.** Schematic of the alloys' preparation process.

The microstructure of the samples was analyzed using optical microscopy (OM) and scanning electron microscopy (SEM), equipped with electron probe microanalysis (JEOL, Tokyo, Japan). X-ray diffraction (XRD) analysis was also conducted using a MAXima XRD-7000 machine equipped with Cu $K\alpha$ radiation on both H-0.4Mg alloy and L-1.4Mg alloy to investigate the effects of Mg concentration on the alloys [28]. The XRD analysis was performed on polished samples and the fixed direction for both samples. Thermo-Calc simulation software equipped with the TCAL8 database was used to calculate the possible amount of each phase that may have developed between 150 and 250 °C [30].

Cyclic polarization tests were conducted to evaluate the corrosion behavior of the alloys in Arabian Gulf seawater. The tests were performed in a three-electrode electrochemical cell using a potentiostat/galvanostat instrument. The working electrode was a polished disc of each alloy with an exposed surface area of 1 cm^2 . A reference electrode made of Ag/AgCl and a counter electrode made of platinum wire were employed in the experiment. Prior to the test, the working electrode surface was cleaned using a series of standard metallographic techniques. The electrochemical cell was filled with Arabian Gulf seawater and maintained at a temperature of 25 °C for 30 min to allow the system to equilibrate. The cyclic polarization test was performed by applying a potential sweep from -0.5 V to $+0.5 \text{ V}$ vs. Ag/AgCl at a scan rate of 1 mV/s . The potential sweep was first conducted in the positive direction (anodic scan), until a current density of $10 \mu\text{A/cm}^2$ was reached, and then in the negative direction (cathodic scan), until the current density returned to the initial value. The potential difference between the working electrode and the reference electrode was recorded throughout the test, and the resulting current–potential curve was used to determine the corrosion behavior of the alloys.

Finally, this methodology is designed to provide comprehensive insights into the mechanical properties and corrosion resistance of the Al–Cu–Mg–Ag alloy as a function of Cu/Mg ratios. The results of this study contribute to the understanding of the behavior of Al–Cu–Mg–Ag alloys in various environments and have practical implications for the selection and use of these alloys in various industrial applications.

3. Results

The hardness comparison of the investigated alloys is presented in Figure 3, which shows that the low Cu/Mg ratio alloy (L-1.4Mg) presents a higher hardness directly after the supersaturated solid solution (SSS) at the onset of the aging process, with a value of 122 Hv. In contrast, the high Cu/Mg ratio alloy (H-0.4Mg) only reached 102 Hv. The explanation for this difference lies in the high concentration of Mg in the low Cu/Mg ratio alloy, leading to the supersaturation of Mg atoms in the aluminum matrix, as indicated by the supersaturated solid solution theory [28]. This results in improved hardness, which continues to improve through the precipitate hardening theory, characterized by the accumulation of alloy elements to form different precipitates. This is due to the diffusion of elements within the alloys, leading to larger precipitates until they reach a uniform size and distribution. The peak hardness values of the L-1.4Mg alloy and H-0.4Mg alloy were 149 Hv and 138 Hv, respectively. Despite initially increasing, the hardness of both alloys eventually started to decrease. However, the hardness of L-1.4Mg was less than the SSS stage after 48 h, which can be attributed to an increment in the size of the θ precipitate relative to the S precipitate. The larger size of precipitates negatively affected the hardness due to an increased mismatch between the aluminum matrix and precipitates [11].

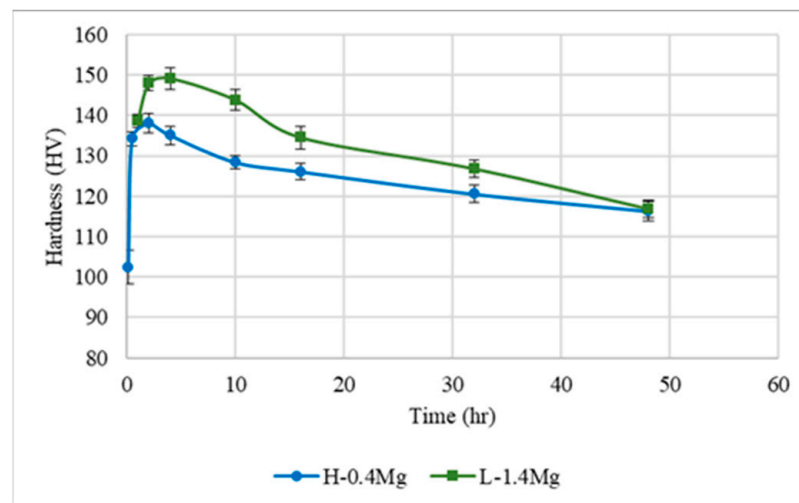


Figure 3. Age-hardening curves of Al–Cu–Mg–Ag alloys with high and low Cu/Mg ratios.

The effect of the high and low Cu/Mg ratios on the tensile test is demonstrated in Figure 4. The results show that a decrease in Mg content leads to an increase in the yield stress from 362 to 381 MPa, or 5%, as well as an increase in the tensile stress from 391 to 426 MPa. However, the low Cu/Mg ratio alloy was found to be brittle, with a percentage ductility of 2 compared to 10 for the high Cu/Mg ratio alloy. This reduction in yield stress, tensile stress, and ductility percentage may be due to the increased size of the precipitates as the Mg content increases, leading to a mismatch between the aluminum matrix and precipitates' clusters. In addition, Figure 5 compared the amounts of the S phase and L-1.4 Mg at 180 °C at the aging temperature, and the Thermo-Calc simulation software [30] supports these observations. In particular, the L-1.4Mg alloy had an average size of 18 μm for the S phase, which is three times larger than the critical size of the S phase (4.5 μm) [31].

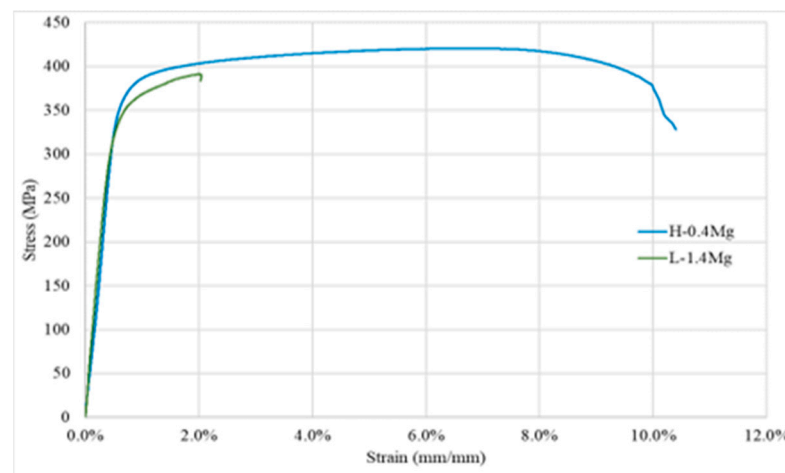


Figure 4. The tensile stress–strain curves of Al–Cu–Mg–Ag alloys with high and low Cu/Mg ratios.

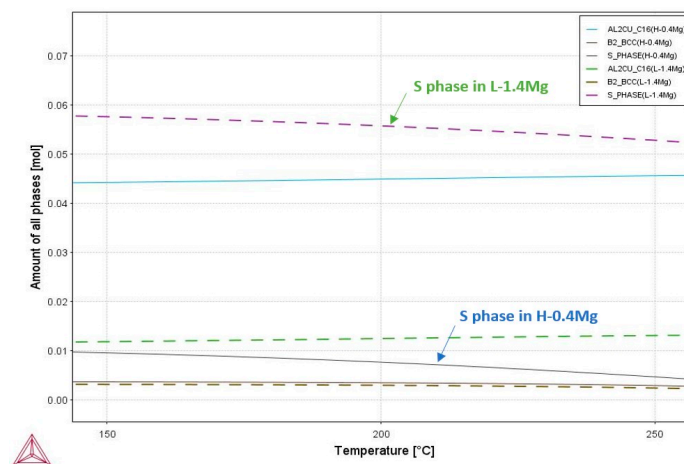


Figure 5. Thermo-Calc simulation showing the amount of S phase in H-0.4Mg alloy and L-1.4Mg alloy at the range of temperature from 150 to 250 °C.

The optical micrograph of Al–Cu–Mg–Ag alloys with high and low Cu/Mg ratios provides valuable insight into the microstructure of the alloys. As shown in Figure 6A, the high Cu/Mg ratio exhibits an average grain size of approximately 205 μm , while the low Cu/Mg ratio, as depicted in Figure 6B, displays an average grain size of 139 μm . According to the findings, the alloys' incorporation of Mg prevents recrystallization from occurring throughout the artificial aging process. The large size of the precipitates in the L-1.4Mg alloy may be responsible for the limited recrystallization size, as indicated by Figure 7. This leads to an increase in the mismatch between the lattice parameters of the alloy matrix and the S phase. In addition, this might affect the tensile result by increasing the average size of the S phase from 3 μm to 18 μm in the high Cu/Mg ratio alloy when the Mg concentration rose from 0.4 to 1.4. This observation is further supported by the X-ray diffraction (XRD) results, which show the presence of large-sized S phases separated at several planes, as shown in Figure 8. XRD results support the increase in Mg content in the L-1.4Mg alloy enhanced the formation of the S phase, as evidenced by the peak XRD at 2θ angles of 24° and 35° . As well, the XRD results show multiple peaks with a high intensity of the S phase in L-1.4Mg compared to H-0.4Mg. The limited recrystallization size can be explained in other ways as well though. Another that might be important is the L-1.4Mg alloy's abundance of Ω phases, which are composed of Al–Cu–Mg–Ag. This, however, is outside the purview of this investigation. Our previous work showed that the mechanical properties of alloys with a high Mg content can be improved by increasing the Ag content, which suggests that the Ω phase may have a negative impact on the recrystallization process [29].

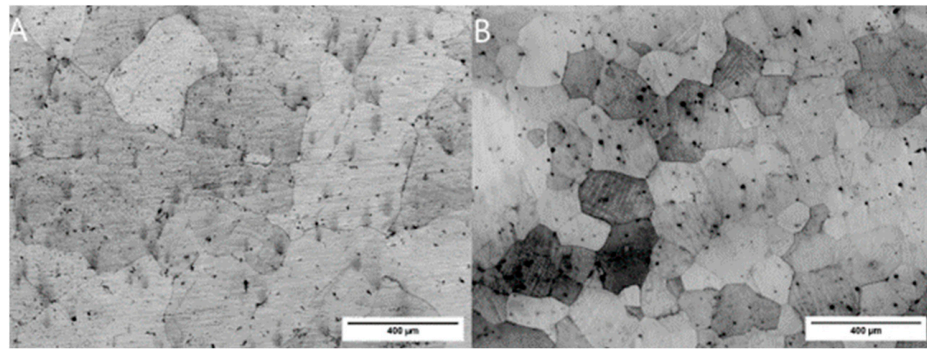


Figure 6. Optical Microscope images of (A) H-0.4Mg alloy and (B) L-1.4Mg alloy.

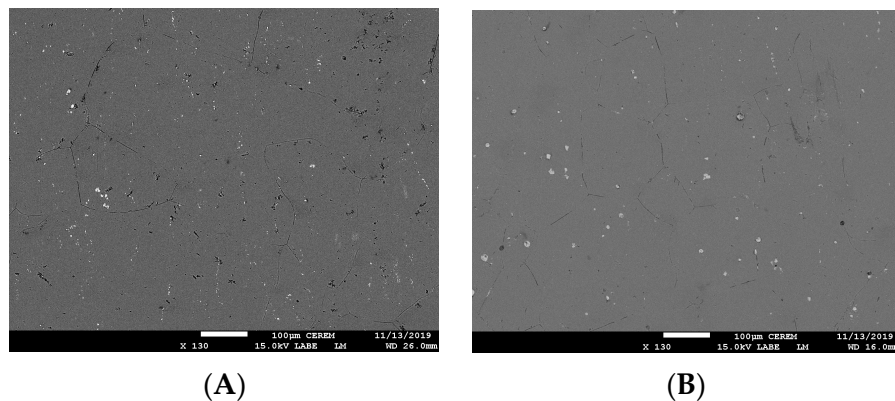


Figure 7. SEM images of alloys to show the S phase size: (A) H-0.4Mg alloy and (B) L-1.4Mg alloy.

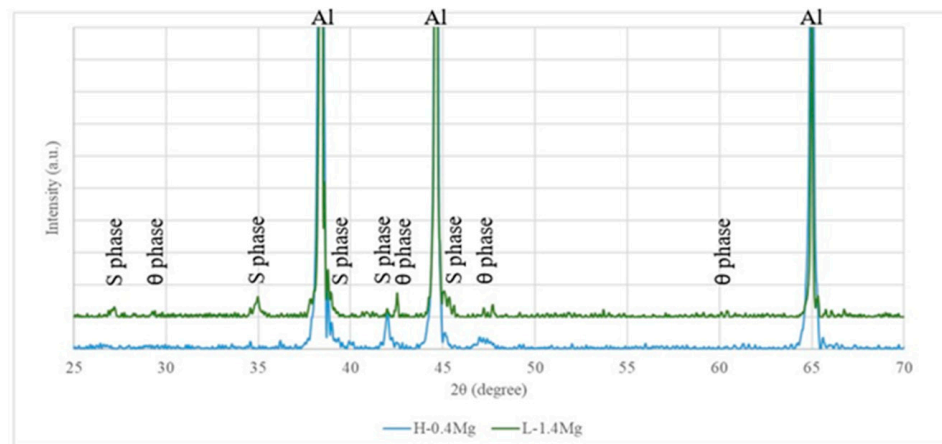


Figure 8. XRD patterns of H-0.4Mg alloy and L-1.4Mg alloy.

The samples were immersed in seawater for 120 h to investigate the corrosion activity on the particles, as shown in Figure 9. The impact of corrosion is dependent on the utilized composition, leading to varying reactions to the corrosion. Based on the image, it appears that corrosion may have begun in the area surrounding the particles, where the mismatch between the Al-matrix and the particles might have a chance. This result is supported by the cycle polarization test, as shown in Figure 10, which shows that the H-0.4Mg has the higher corrosion potential, while the L-1.4Mg has the lower corrosion potential. However, the particle size might be involved in the corrosion rate, where the L1.4Mg alloy has the bigger particle size, which enhances the corrosion rate compared to the small particle size in the H-0.4Mg alloy.

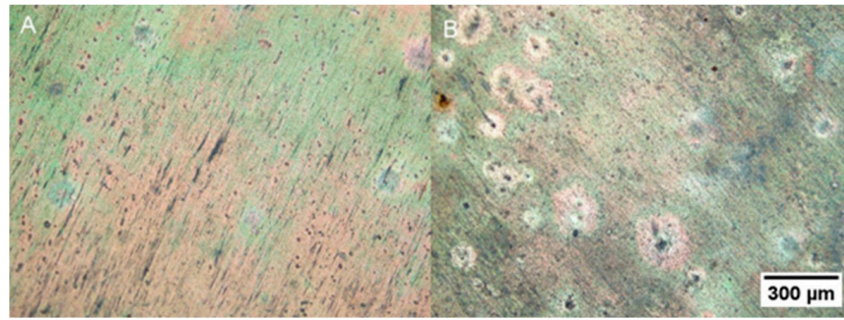


Figure 9. Optical Microscope images of the samples immersed for 120 h in Arabian Gulf seawater: (A) H-0.4Mg alloy and (B) L-1.4Mg alloy.

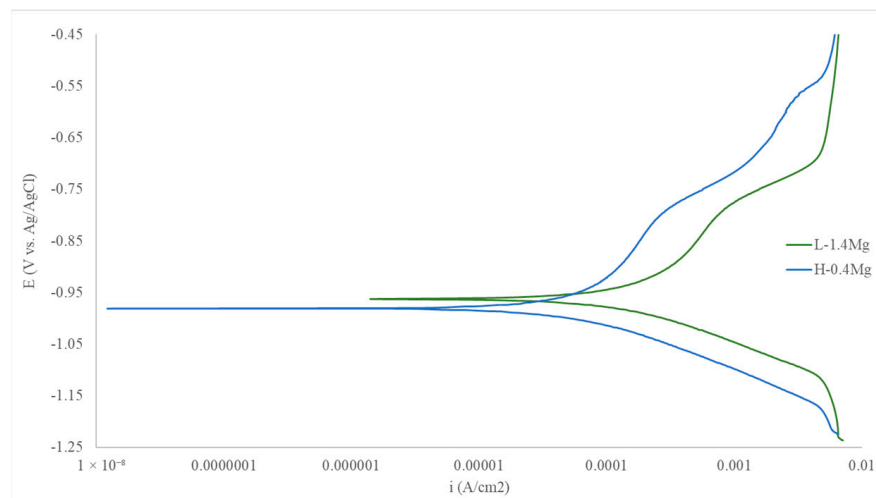


Figure 10. Cycle polarization curves of alloys' (H-0.4Mg alloy and L-1.4Mg alloy) immersion for 30 min in Arabian Gulf Seawater.

4. Discussion

The results section illustrates that Mg concentration has a significant influence on Al–Cu–Mg–Ag alloys, as summarized in Table 2. Despite increasing the material's hardness, Mg reduces yield stress and ductility. The XRD results and Thermo-Calc simulation were used to identify the phases that formed on the alloys during the aging process. It is evident that the S phase played a crucial role. It was dependent not only on the S phase quantity in the bulk but also on the phase size. The hardness result indicates that a high Mg content increases the hardness of the alloy, while decreasing the yield stress and ductility. This is due to the increased size of the S phase, which increased the mismatch between the S phase and the Al matrix. The result of the ductility can confirm this. Compared to a lower Mg content, a higher Mg content produced finer grains. In general, a high Mg content is expected to produce a higher yield stress, contingent upon the Hall–Petch strengthening theory. However, this resulted in a comparison of the grain size to the particle size. The argument is supported by the proportion of the grain size to the particle size. The percentage of high Mg content was approximately 8%, while the percentage of low Mg content was 68%. This huge disparity in the grain-to-particle ratio justifies the effect of the particle size on the strength of the alloy. Nonetheless, the particle size inhibited recrystallization during the artificially aged process, even when the Mg content was doubled. This was due to the effect of the particle size on the process of recrystallisation. Based on the Mg corrosion ability, it was anticipated that a higher Mg content would increase the corrosion activity, as shown in Figure 10. The corrosion activity was reduced due to the large particle size in the high Mg content alloy, which decreased the contact surface with the medium. Furthermore,

the S phase particle-strengthening contribution was analyzed for both alloys by using the Orowan strengthening model, as follows:

$$\sigma_p = M \frac{0.4Gb}{\pi\sqrt{1-\nu}} \frac{\ln(2 * \bar{r}/b)}{\lambda_p} \quad (1)$$

where M is the Taylor factor for the FCC, which is 3.06 for Al; G is the shear modulus, 26.9 GPa; b is the magnitude of the Burgers vector, 0.286 nm; ν is the Poisson ratio, 0.33; \bar{r} is the mean radius of the spherical precipitate in a circular cross section = $\sqrt{2/3} * r$; r is the average particle radius; and λ_p is the average inter-particle spacing. The λ_p can be estimated from the following Equation [32]:

$$\lambda_p = 2\bar{r} \left(\sqrt{\frac{\pi}{4f}} - 1 \right) \quad (2)$$

where f is the volume fraction of the particles.

Table 2. Summary of the results showing the effect of Cu/Mg ratio.

Alloy	H-0.4Mg	L-1.4Mg
YS (MPa)	381 ± 11	362 ± 10
UTS (MPa)	426 ± 13	391 ± 7
% Ductility	10 ± 2	2 ± 0.6
Hardness (HV)	138 ± 2	149 ± 3
Grain size (µm)	205 ± 7	139 ± 5
Particle size (µm)	3	18
% Grains/Particles	68	7.72
Peak aging time (h)	2	4
E (V vs. Ag/AgCl)	−0.99	−0.96

The contribution of the S phase in both alloys was calculated, and it was found that the S phase contributed to yield strength by 35 MPa in the H-0.4Mg alloy, where there was a negative effect of the S phase in the L-1.4Mg alloy.

5. Conclusions

This study aimed to investigate the effect of magnesium content on the properties of Al–Cu alloys, which is summarized by the following points:

1. The results showed that magnesium (Mg) has a significant impact on Al–Cu alloys, with increasing Mg content leading to increased hardness but reduced yield stress and ductility.
2. The results indicated that a high Mg content resulted in finer grains and a larger S phase size, which caused a mismatch between the S phase and the aluminum matrix, leading to reduced yield stress and ductility.
3. The grain-to-particle size ratio was found to be crucial in determining the strength of the alloy, with a high Mg content having a smaller ratio compared to a low Mg content.
4. The particle size was found to inhibit grain growth during the artificial aging process, even when the Mg content was doubled.
5. Despite being known for its corrosion ability, a high Mg content reduced corrosion activity due to the large particle size in the high Mg content alloy.
6. As for future work, reducing the S phase size in the high Mg content might be useful in improving the properties of the Al–Cu–Ag alloys and the coherency of the S phase.

Overall, this study provides valuable insights into the impact of Mg on Al–Cu–Ag alloys and highlights the importance of further ways to explore reducing the S phase size

in the high Mg content to improve the material's properties. In addition, a deep study of an Ag effect on the alloy might be useful in future work.

Author Contributions: T.T.A. formulated the experimental design, analyzed the experimental data, and wrote the original draft; M.F.I., H.F.A. and M.S.S. discussed the results and made the revisions. All authors have read and agreed to the published version of the manuscript.

Funding: Researchers Supporting Project number RSPD2023R579, King Saud University, Riyadh, Saudi Arabia.

Data Availability Statement: If needed, the corresponding author can provide access to the datasets generated and/or analyzed during the current study upon request that is deemed reasonable.

Acknowledgments: The authors extend their appreciation to the Researchers Supporting Project number RSPD2023R579, King Saud University, Riyadh, Saudi Arabia.

Conflicts of Interest: The authors declare no conflict of interest.

References

1. Kaufman, J.G. *Introduction to Aluminum Alloys and Tempers*; ASM International: Materials Park, OH, USA, 2000.
2. Muddle, B.C.; Polmear, I.J. The Precipitate Ω Phase in Al-Cu-Mg-Ag Alloys. *Acta Metall.* **1989**, *37*, 777–789. [[CrossRef](#)]
3. Porter, D.A.; Easterling, K.E.; Sherif, M.Y. *Phase Transformations in Metals and Alloys*, 3rd ed.; CRC Press: Boca Raton, FL, USA, 2009; ISBN 9781439883570.
4. Bai, S.; Liu, Z.; Gu, Y.; Zhou, X.; Zeng, S. Microstructures and Fatigue Fracture Behavior of an Al-Cu-Mg-Ag Alloy with a Low Cu/Mg Ratio. *Mater. Sci. Eng. A* **2011**, *530*, 473–480. [[CrossRef](#)]
5. Wang, S.C.; Starink, M.J. Two Types of S Phase Precipitates in Al-Cu-Mg Alloys. *Acta Mater.* **2007**, *55*, 933–941. [[CrossRef](#)]
6. Starink, M.J.; Yan, J.L. Precipitation Hardening in Al-Cu-Mg Alloys: Analysis of Precipitates, Modelling of Kinetics, Strength Predictions. In *Materials Science Forum*; Trans Tech Publications Ltd.: Stafa-Zurich, Switzerland, 2006.
7. Wang, S.C.; Starink, M.J.; Gao, N. Overview of Recent Work on Precipitation in Al-Cu-Mg Alloys. In *Materials Science Forum*; Trans Tech Publications Ltd.: Stafa-Zurich, Switzerland, 2007.
8. Feng, Z.; Yang, Y.; Huang, B.; Han, M.; Luo, X.; Ru, J. Precipitation Process along Dislocations in Al-Cu-Mg Alloy during Artificial Aging. *Mater. Sci. Eng. A* **2010**, *528*, 706–714. [[CrossRef](#)]
9. Zuniga, A. Microstructure and Aging Behavior of Conventional and Nanocrystalline Aluminum-Copper-Magnesium Alloys with Scandium Additions. Ph.D. Thesis, University of California, Davis, CA, USA, 2006.
10. Liu, J.-Z.; Wang, S.; Wu, C.; Liu, J.Z.; Yang, S.S.; Wang, S.B.; Chen, J.H.; Wu, C.L. The Influence of Cu/Mg Atomic Ratios on Precipitation Scenarios and Mechanical Properties of Al-Cu-Mg Alloys. *J. Alloys Compd.* **2014**, *613*, 139–142. [[CrossRef](#)]
11. Ardell, A.J. Precipitation Hardening. *MTA* **1985**, *16*, 2131–2165. [[CrossRef](#)]
12. Campbell, F.C. *Elements of Metallurgy and Engineering Alloys*; ASM International: Materials Park, OH, USA, 2008.
13. Murayama, M.; Hono, K. Three Dimensional Atom Probe Analysis of Pre-Precipitate Clustering in an Al-Cu-Mg-Ag Alloy. *Scr. Mater.* **1998**, *38*, 1315–1319. [[CrossRef](#)]
14. Knowles, K.M.; Stobbs, W.M. The Structure of {111} Age-Hardening Precipitates in Al-Cu-Mg-Ag Alloys. *Acta Crystallogr. Sect. B Struct. Sci.* **1988**, *44*, 207–227. [[CrossRef](#)]
15. Kerry, S.; Scott, V.D. Structure and Orientation Relationship of Precipitates Formed in Al-Cu-Mg-Ag Alloys. *Met. Sci.* **2013**, *18*, 289–294. [[CrossRef](#)]
16. Kazanjian, S.M.; Wang, N.; Starke, E.A. Creep Behavior and Microstructural Stability of Al-Cu-Mg-Ag and Al-Cu-Li-Mg-Ag Alloys. *Mater. Sci. Eng. A* **1997**, *234–236*, 571–574. [[CrossRef](#)]
17. Chen, Y.T.; Nieh, G.Y.; Wang, J.H.; Wu, T.F.; Lee, S.L. Effects of Cu/Mg Ratio and Heat Treatment on Microstructures and Mechanical Properties of Al-4.6Cu-Mg-0.5Ag Alloys. *Mater. Chem. Phys.* **2015**, *162*, 764–770. [[CrossRef](#)]
18. Ringer, S.P.; Yeung, W.; Muddle, B.C.; Polmear, I.J. Precipitate Stability in Al Cu Mg Ag Alloys Aged at High Temperatures. *Acta Metall. Mater.* **1994**, *42*, 1715–1725. [[CrossRef](#)]
19. Bai, S.; Ying, P.; Liu, Z.; Wang, J.; Li, J. Quantitative Transmission Electron Microscopy and Atom Probe Tomography Study of Ag-Dependent Precipitation of Ω Phase in Al-Cu-Mg Alloys. *Mater. Sci. Eng. A* **2017**, *687*, 8–16. [[CrossRef](#)]
20. Ringer, S.P.; Sakurai, T.; Polmear, I.J. Origins of Hardening in Aged Al-Cu-Mg-(Ag) Alloys. *Acta Mater.* **1997**, *45*, 3731–3744. [[CrossRef](#)]
21. Gable, B.M.; Shiflet, G.J.; Starke, E.A. The Effect of Si Additions on Ω Precipitation in Al-Cu-Mg-(Ag) Alloys. *Scr. Mater.* **2004**, *50*, 149–153. [[CrossRef](#)]
22. Chang, Y.C.; Howe, J.M. Composition and Stability of Ω Phase in an Al-Cu-Mg-Ag Alloy. *Metall. Trans. A* **1993**, *24*, 1461–1470. [[CrossRef](#)]
23. Ünlü, N.; Gable, B.M.; Shiflet, G.J.; Starke, E.A. The Effect of Cold Work on the Precipitation of Ω and Θ in a Ternary Al-Cu-Mg Alloy. *Metall. Mater. Trans. A Phys. Metall. Mater. Sci.* **2003**, *34*, 2757–2769. [[CrossRef](#)]

24. Ringer, S.P.; Hono, K.; Polmear, I.J.; Sakurai, T. Nucleation of Precipitates in Aged AlCuMg(Ag) Alloys with High Cu:Mg Ratios. *Acta Mater.* **1996**, *44*, 1883–1898. [[CrossRef](#)]
25. Wang, J.; Liu, Z.; Bai, S.; Cao, J.; Zhao, J.; Zeng, D. Combined Effect of Ag and Mg Additions on Localized Corrosion Behavior of Al-Cu Alloys with High Cu Content. *J. Mater. Eng. Perform.* **2020**, *29*, 6108–6117. [[CrossRef](#)]
26. Qi, H.; Liu, X.Y.; Liang, S.X.; Zhang, X.L.; Cui, H.X.; Zheng, L.Y.; Gao, F.; Chen, Q.H. Mechanical Properties and Corrosion Resistance of Al-Cu-Mg-Ag Heat-Resistant Alloy Modified by Interrupted Aging. *J. Alloys Compd.* **2016**, *657*, 318–324. [[CrossRef](#)]
27. Liu, X.Y.; Wang, Z.P.; Fu, B.G.; Long, L.; Zhang, X.L.; Cui, H.X. Effects of Mg Content on the Mechanical Properties and Corrosion Resistance of Al-Cu-Mg-Ag Alloy. *J. Alloys Compd.* **2016**, *685*, 209–215. [[CrossRef](#)]
28. Ijaz, M.F.; Soliman, M.S.; Hashmi, F.H.; Alasmari, A.S.; Abbas, A.T. Comparison of Mechanical and Microstructural Properties of As-Cast Al-Cu-Mg-Ag Alloys: Room Temperature vs. High Temperature. *Crystals* **2021**, *11*, 1330. [[CrossRef](#)]
29. Alshammari, T.T.; Alharbi, H.F.; Soliman, M.S.; Ijaz, M.F. Effects of Mg Content on the Microstructural and Mechanical Properties of Al-4Cu-XMg-0.3Ag Alloys. *Crystals* **2020**, *10*, 895. [[CrossRef](#)]
30. TCS. *Al-Based Alloy Database (TCAL8)*; Thermo-Calc Software AB: Stockholm, Sweden, 2022.
31. Zhao, Q.; Liu, Z.; Li, S.; Hu, Y.; Bai, S. Effect of S Phase Characteristics on the Formation of Recrystallization Textures of an Al-Cu-Mg Alloy. *J. Alloys Compd.* **2018**, *747*, 293–305. [[CrossRef](#)]
32. Zhu, Z.; Ng, F.L.; Seet, H.L.; Lu, W.; Liebscher, C.H.; Rao, Z.; Raabe, D.; Mui Ling Nai, S. Superior mechanical properties of a selective-laser-melted AlZnMgCuScZr alloy enabled by a tunable hierarchical microstructure and dual-nanoprecipitation. *Mater. Today* **2022**, *52*, 90–101. [[CrossRef](#)]

Disclaimer/Publisher’s Note: The statements, opinions and data contained in all publications are solely those of the individual author(s) and contributor(s) and not of MDPI and/or the editor(s). MDPI and/or the editor(s) disclaim responsibility for any injury to people or property resulting from any ideas, methods, instructions or products referred to in the content.